# A Computational Method Involving Surface Area to Volume Ratio to Estimate Inorganic Nanoparticle Efficacy

**Wesley A. Williams[1,2,*], Ashley J. Denslow[1,2], Peter W. Radulovic[1,2], Daniel J. Denmark [1,2], and Shyam S. Mohapatra[1,2,3,4]**

[1]  Graduate Programs, Taneja College of Pharmacy, University of South Florida, Tampa, FL;
[2]  USF Division of Translational Medicine and Center for Research and Education in Nanobioengineering, University of South Florida, Tampa, FL;
[3]  Department of Internal Medicine, Morsani College of Medicine, University of South Florida, Tampa, FL;
[4]  James A Haley VA Hospital, Tampa, FL;
[*]  Correspondence: smohapat@usf.edu and wesleyallenwilliams@usf.edu

**Abstract:**   Inorganic nanoparticles are utilized for therapeutic, diagnostic, or theranostic purposes and the latter involve simultaneous sensing, imaging, or tracking of drug delivery. Further, these nanoparticles differ in their morphologies, which affect outcomes such as the effectiveness of hyperthermia, induction, drug loading, circulation time by escaping the body's immune system, imaging modality clarity, and biosensing. However, design of these theranostics is limited by the lack of a method to predict their therapeutic efficacy. Herein, we report a computational approach involving the surface area (SA) to volume (V) ratios (SA:V), which can help predict the efficacy of the inorganic nanoparticles. The approach comprises a coding platform for the comparator program and uses a Python 3 on a Windows 10 operating system. Analyses of 22 polyhedral morphologies that inorganic nanoparticles could assume ex silico showed that only particular concave morphologies in this size regime are more productive over the standard sizes. Our results provide a method that can aid in the predicting efficacy of inorganic nanoparticles with certain morphology.

**Keywords:** inorganic nanoparticles; in silico; optimization; theranostic; therapeutic; diagnostic; computation; coding; Python

## 1. Introduction

Inorganic nanoparticles have been used across three main nanotherapeutic modes as a methodology for optimizing medicine and testing in terms of cost, ease of use, accessibility, and toxicity: therapeutic, diagnostic, and theranostic. In a therapeutic sense, these nanoparticles can have their surface chemistry altered for conjugating drug payloads and biological molecules onto them for drug delivery, offering antimicrobial measures of protection, and even as vaccine carriers (Pfizer/BioNTech's and Moderna's SARS-CoV-2 nano vaccines) [1,2]. In the diagnostic sense, these nanoparticles can serve as label-free contrast agents that produce a higher resolution image of cancers that may escape traditional metal-based dyes. They can also serve as sensors that monitor levels of key diagnostic biomarkers in human sera (like molecularly imprinted nanoparticles for point-of-care-testing (POCT)), potentially facilitating high-level care more ubiquitously in comparison to traditional testing via their selectivity for specific target molecules. Their reusability, sensitivity through increasing conduction physiochemically, portability, and reproducibility all aid in that endeavor and purpose [3]. Lastly, in the theranostic sense, these nanoparticles, in addition to identifying cancerous cells via imaging, can exact localized hyperthermia without inducing damaging thermal ablation via alternating magnetic frequencies due to the paramagnetic or superparamagnetic nature of the metal/metal oxides they are composed from. One such example uses superparamagnetic iron-oxide nanoparticles (SPIONs) encased in a photopolymerizable substance poly-N-isopropylacrylamide (PNIPAM) that can release these nanoparticles on exposure to an alternating magnetic

field, ensuring a more optimized usage and less ability to agglomerate and trigger an immune response [4-6].

Inorganic nanoparticles can be fabricated in a variety of morphologies, like those shown in Table 1. Tuning inorganic nanoparticles in a physical sense allows researchers to increase their efficiency with ease, allowing them to improve their absolute loading capability and efficiency, magnetizability, and increased reactivity making them more prone to interact with biological contaminants as an antibiotic electrochemically. For example, Kordashenas and Ghorbani reported the reactivities of different morphological applications of silver nanoparticles like the cube, sheet, and near-spheroid nanoparticle elucidating that a significant increase in efficacy is shown sequentially, giving a potential rise as a nanoformulation made for antimicrobial purposes alone [7]. Furthermore, increasing the particle's surface area (SA) to volume (V) ratio (SA:V) at a standardized size was used to investigate the efficacy of different morphologies effects on nanotoxicology [8]. Moreover, octahedral iron oxide nanoparticles were shown to enhance magnetically induced hyperthermia even more so than traditionally spheroid nanoparticles [9].

Nanoparticles with diverse morphologies were produced by different chemical means from the bottom up via crystallization or seeded-nucleation techniques [10]. Thus, Thambi and associates reported creating multiple morphologies for gold nanorods by changing the concentration of silver nitrate in the presence of varying pH levels, most notably for creating octahedral nanoparticles [11]. Also, an approach for octahedral nanoparticles and other morphologies such as truncated cubes, cuboctahedra, and truncated octahedra were reported to develop as the plane encompassing the x, y, and z direction is formed at different convective solvent flows and vertex truncation [12]. Furthermore, a bottom-up process of core-shell type Pt-Pd icosahedral nanoparticle formulation that implements multiphase (air/liquid) microfluidics employing sodium tetrachloropalladate ($Na_2PdCl_4$) and PVP dispersed diethylene glycol solution was reported [13]. Moreover, a method of creating concave polyhedral specifically tris-octahedral nanoparticles, was shown by adding a higher concentration of reductants (like halide anions), which tempered the formation of gold nanoparticles with desired morphology [14]. Also, the methodologies for creating multiple types of morphologies including icosidodecahedral, dodecahedral, and tetrahedral inorganic particles using seeded-growth (former two)/oleylamine-mediated protocols has been reviewed [15].

In addition to above referred bottom-up approaches several top-down approaches have been investigated. A recent review details the popular methods, such as the optical lithography, a nanofabrication tool with longevity that can quickly form 3D structure at decent resolutions in a high throughput manner. The only issue is that there is a tradeoff that must be decided between resist sensitivity and resolution. E-beam lithography allows etching of small features less than 20 nm in dimension. Unfortunately, it is a highly expensive and low throughput process that cannot create features less than 5 nanometers. Another method involves soft/nanoimprint lithography, which is a simple pattern transfer based nanofabrication tool capable of etching features less than 10 nm but has a disadvantage with its low-throughput process being unable to make densely-packed nanostructures (low periodicity). Moreover, it is costly and dependent on other means for template creation. Block co-polymer lithography is a high-throughput, low-cost method for mass producing nanostructures like spheres and cylinders but possesses issues with periodicity. Lastly, and arguably the most efficacious, scanning probe lithography can be employed: a high-resolution chemical, molecular, and mechanical nanopatterning method that has the capability of manipulating individual atoms. The caveat lies in not being a high throughput process, has a high expense, and requires an ultra-high-vacuum based version [16].

Despite extensive research in this field which of the diverse morphologies can yield efficient nanoparticles remains a major limitation of the field. To meet this unmet need herein we undertook an investigation of 22 polyhedral morphologies that inorganic nanoparticles could assume ex silico.  We show that estimation of physical properties of

these nanoparticles, such as SA:V by a computational approach, provides a key index for which the functional efficacy of inorganic nanoparticles can be measured.

## 2. Materials and Methods

**The Processor:** The processor native to the 64-bit operating system is the Intel(R) Core(TM) i3-1005G1. The size of the RAM at 12.0 GB was sufficient for multiple processes. The operating system is Windows 10 Home.
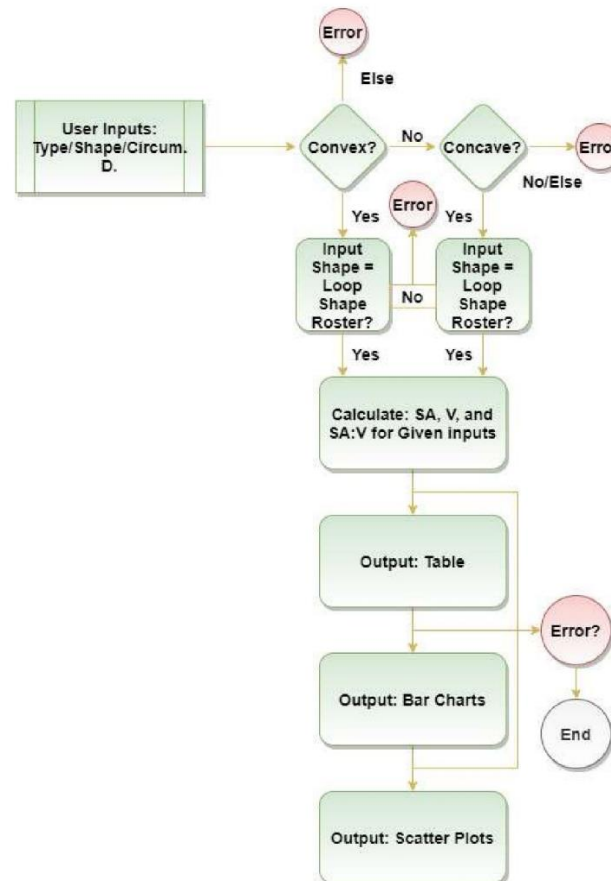
**Figure 1.** Logic of Comparator Code

**Python:** The version of Python used for the program was version: 3.8.5. The anaconda application was used to consolidate the necessary packages with the Jupyter Notebook application as the coding interface. The "Math" package was used for simple mathematical functions used for SA:V calculations in the program and "NumPy" for data manipulation into arrays for plotting. "Matplotlib pyplot" was used for plotting the resulting data of the 22 shapes across the nano-regime. Finally, "Tabulate" was used for creating the table of values calculated for each shape's SA:V at 10 nm.

Figure 1 describes the logic of our algorithm. The beginning of the code requires three user inputs that determine the outcome of the initial outputs via conditional loops. The polyhedron's name, type (concave or convex), and the circumsphere diameter a researcher wants to investigate are required. Clerical mistakes and the like trip the error and terminate the loop and the program altogether. If not, the surface area, volume, and surface area to volume ratio are calculated via mathematical derivations that equate concave polyhedra parameters as if they were convex polyhedra (details for derivations described in the Supplemental Information section).

Next, the conditional loops are exited when the input conditions are given, and the calculations are outputted. Tables 2 and 3 and Figures 2 and 3 are outputted comparing the SA:V ratio of the various polyhedra investigated from the chosen circumsphere diameter and against the entire nano-regime in Figure 3. Figures 2 and 3 give visual comparisons within subgroups within convex and concave grouping against the standard

circumsphere (exception for "deltoidal icositetrahedron" (mid sphere radius equation is closest to circumsphere radius versus the insphere radius equation).

**Statistical Analysis**. An unpaired two-sample t-test was used. The Tables were formatted from the analysis performed using Excel and the add-in: "Analysis ToolPak".

### 3. Results

To investigate SA :V relationship, the morphology of several convex and concave polyhedra was selected. These included convex polyhedra such as, platonic, Archimedes, Catalan, and concave polyhedra such as Kepler-Poinsot, Da Vinci and Wenninger (Ref) Table 1 shows the 22 polyhedra investigated [17-22].

**Table 1.** Morphology of convex and concave polyhedra investigated: **Convex**: Tetrahedron-Dodecahedron: *Platonic,* Cuboctahedron.-Truncated Octahedron: *Archimedes,* and Deltoidal Icositetrahedron: *Catalan.* **Concave**: Great Dodeca-Small-Stellated Dodecahedron: *Kepler-Poinsot,* Stellated Octahedron.: *Da Vinci,* and Medial Rhombic Triacontahedron-Excavated Dodecahedron: *Wenninger* (Abstract-Regular) [17,18,19,20,21,22].

As can be seen, many of these shapes possess unique morphologies that can optimize the nanoparticle's performance. Nearer the morphology of a sphere or spheroid nanoparticle would leave the observer to infer that their ratios are more similar in comparison to those with more dramatic constructs.

The first output from the program is a tabulation of all of the calculations required for SA:V for each nanoparticle morphology. From inference alone it is to be expected that shapes such as the deltoidal icositetrahedron possess an SA:V closer to a sphere than the stellated octahedron whose concavity offers more surface area against its volume at a

standard diameter. For convex shapes, the number of faces on a shape seem to diminish any gain in SA:V over a sphere expectedly as, from a mathematical standpoint, it is known that as one takes the limit where the number of sides approaches infinity brings a regular polygon closer to the shape of circle in the 2D sense, whereas here, the application of that limit shifts up into the third dimension with the number of faces. We see this concept well in the tetrahedron versus the rhombicuboctahedron, for example, where number of faces sacrifices surface area in the latter's case along with the icosahedron and the Archimedes solids.

**Table 2.** Tabulation of SA, V, and SA:V for all convex shapes with respect to input circumsphere diameter of 10 nm (reference sphere).

| Convex Shape (Abbrev.) | Type | SA (X $10^{-16}$ m$^2$) | V (X $10^{-25}$ m$^3$) | SA:V (X $10^9$) |
|---|---|---|---|---|
| Tetrahedron (TE) | Platonic | 1.15 | 0.64 | 1.80 |
| Octahedron (OCT) | Platonic | 1.73 | 1.67 | 1.04 |
| Icosahedron (IC) | Platonic | 2.39 | 3.17 | 0.76 |
| Cube (CU) | Platonic | 2.00 | 1.92 | 1.04 |
| Dodecahedron (DO) | Platonic | 2.63 | 4.78 | 0.55 |
| Cuboctahedron (CO) | Archimedes | 2.37 | 2.95 | 0.80 |
| Rhombicuboctahedron (RCO) | Archimedes | 2.74 | 3.98 | 0.69 |
| Snub Cube (SCU) | Archimedes | 2.75 | 4.06 | 0.68 |
| Snub Dodecahedron (SDO) | Archimedes | 6.65 | 15.30 | 0.44 |
| Rhombicosidodecahedron (RIDO) | Archimedes | 2.97 | 4.67 | 0.64 |
| Truncated Octahedron (TOCT) | Archimedes | 2.68 | 3.58 | 0.75 |
| Deltoidal Icositetrahedron (DIT)* | Catalan | 3.15 | 4.90 | 0.64 |
| Sphere (SP) REF. | N/A | 3.14 | 5.24 | 0.60 |

* midsphere radius equation is closest to circumsphere radius versus the insphere radius equation

Similarly, the number of faces can reduce this concept in the concave group in terms of preserved volume as evidenced by comparing the Wenninger solids with Da Vinci. Moreover, the length of a vertex to the intersection of the face in concavity contributes beneficially to a higher SA:V so long as the previous detriment is kept into consideration. We see this evidenced within Wenninger's group for the Dodecadodecahedron and small ditrigonal icosidodecahedron and comparison to the medial triambic icositetrahedron. The excavated dodecahedron is a remarkable case in which parts of a regular dodecahedron are cut in a regular fashion offering a substantial amount of surface area but sacrificing major volume.

**Table 3.** Tabulation of SA, V, and SA:V for all concave shapes with respect to input circumsphere diameter of 10 nm (reference sphere).

| Concave Shape (Abbrev.) | Type | SA ($\times 10^{-16}$ m$^2$) | V ($\times 10^{-25}$ m$^3$) | SA:V ($\times 10^9$) |
|---|---|---|---|---|
| Great Dodecahedron (GDO) | Kepler-Poinsot | 3.01 | 2.25 | 1.34 |
| Great Icosahedron (GIC) | Kepler-Poinsot | 2.92 | 0.91 | 3.20 |
| Great-Stellated Dodecahedron (GSDO) | Kepler-Poinsot | 5.05 | 2.37 | 2.13 |
| Small-Stellated Dodecahedron (SSDO) | Kepler-Poinsot | 1.86 | 1.39 | 1.34 |
| Stellated Octahedron (SOCT) | Da Vinci | 0.11 | 0.02 | 7.20 |
| Medial Rhombic Triacontahedron (MRT) | Abstract-Regular (Wenninger) | 4.14 | 3.67 | 1.20 |
| Dodecadodecahedron (DODO) | Abstract-Regular (Wenninger) | 1.10 | 2.57 | 0.43 |
| Medial Triambic Icosahedron (MTIC) | Abstract-Regular (Wenninger) | 1.47 | 0.33 | 4.44 |
| Small Ditrigonal Icosidodecahedron (SDIDO) | Abstract-Regular (Wenninger) | 1.44 | 3.36 | 0.43 |
| Excavated Dodecahedron (EDO) | Abstract-Regular (Wenninger) | 3.31 | 0.19 | 17.00 |
| Sphere (SP) | N/A | 3.14 | 5.24 | 0.60 |

Note that for the Deltoidal Icositetrahedron in the convex group the mid-sphere was calculated in absence of a calculation for the circumsphere, offering a slight discrepancy in standardization due to the nature of the polyhedron. It must also be taken into account that, for a specific application, the volumes of these nanoparticles at a standard size should be recognized despite high SA:V. Again, the excavated dodecahedron looks attractive as well as the stellated octahedron but offers significantly less volume. While offering greater ability of surface modification and induction, this may be detrimental if the material itself needs to be at an adequate mass for the therapy or diagnostic capability. Surface area and volume should be weighed with importance and consideration in addition.

Consistent with the previous tabulations, Figures 2 and 3 reveal insightful differences in SA:V against shapes within subgroups when compared to the reference sphere. The tetrahedron offers a significantly considerable amount of SA:V for nanoformulation of a standard size. The cuboctahedron, rhombicuboctahedron, and truncated octahedron offer a significantly higher SA:V within their group though globally the significance is lost. However, what is not observed is a palpable difference in inefficacies between shapes. For the Kepler-Poinsot, the great icosahedron outperformed the rest though the whole offers significance against the reference sphere. For the Wenninger, we see the highest significance for the excavated dodecahedron but the aforementioned considerations still hold.
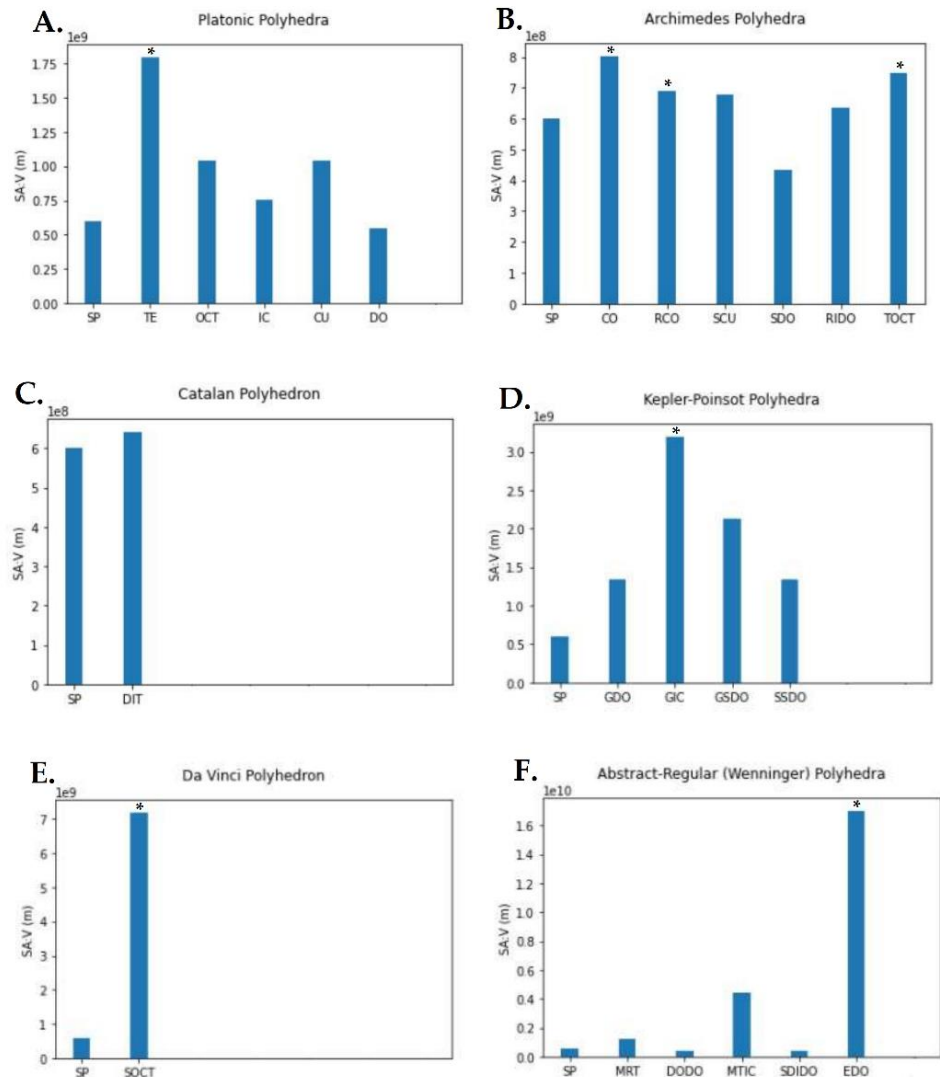
**Figure 2.** SA:V, measured in m$^{-1}$, as a function of morphology for the **A.** Platonic, **B.** Archimedes, **C.** Catalan, **D.** Kepler-Poinsot, **E.** Da Vinci, and **F.** Wenninger polyhedra. Note the multiplicative scaling factor is given at the top of the SA:V axis (Asterisks denote "experimenter's mean or chosen value" that breaches significance on unpaired 2-sample t-tests).

Significant SA:V differences are observed for nanoparticles smaller than 20 to 30 nm, with the highest efficacy exhibited for nanoparticles less than 10 nm circumsphere diameter. The differential significance rate is logarithmically proportional and increases towards the picometer regime, similar to the last proportions of SA:V within subgroups. Note that the ratios of the octahedron and cube against the circumsphere are equal thus the missing curve for the octahedron is from the program's output by happenstance. Shapes with the most dramatic divergence indicate an even greater potential of efficacy.
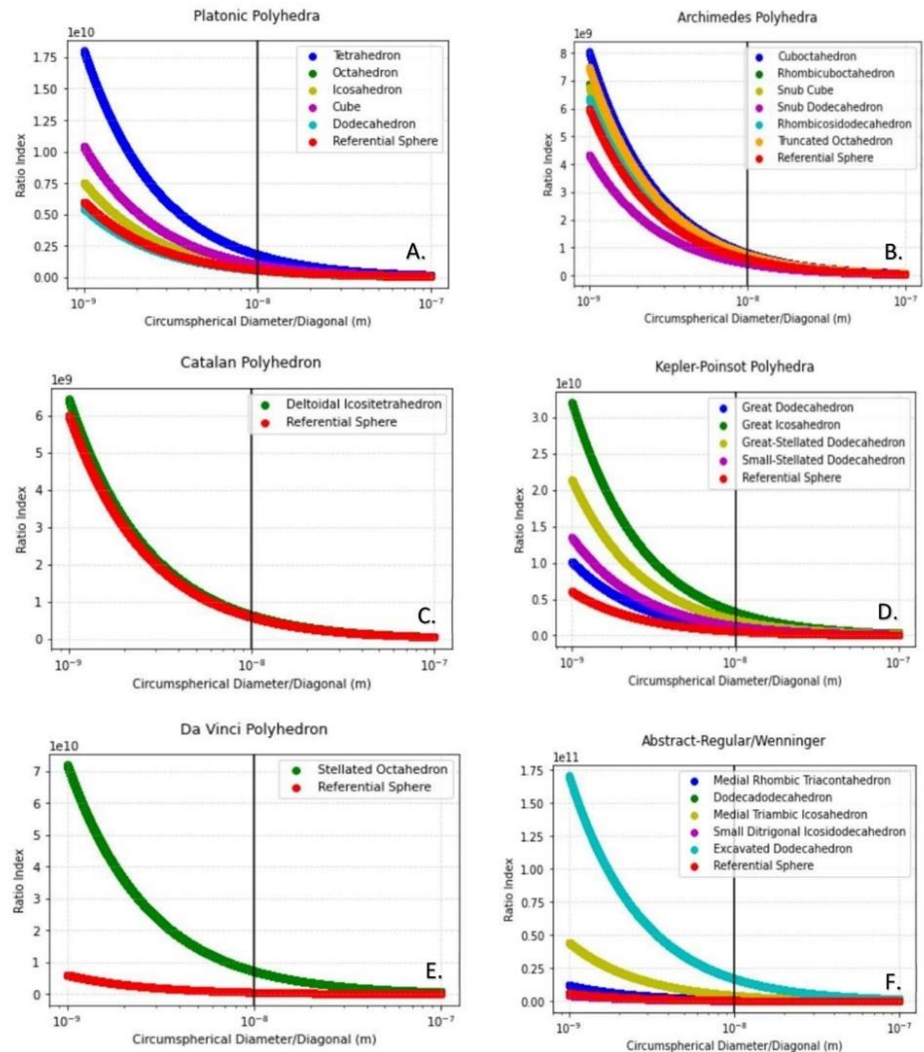
**Figure 3.** Six-panel scatter plot of SA:V, measured in m⁻¹, as a function of morphology across the nano-regime for the **A.** Platonic, **B.** Archimedes, **C.** Catalan, **D.** Kepler-Poinsot, **E.** Da Vinci, and **F.** Wenninger polyhedra. *Note the multiplicative scaling factor is given at the top of the SA:V axis.

From a statistical standpoint, the previous graphs indicate significance with respect to their respective groups determined by an unpaired two-sample t-test to indicate statically significant differences in SA:V against the reference sphere, as seen in Table 4. It was found that only the Kepler-Poinsot polyhedra group was significantly different than the other three groups (fashioned by combing the single-shaped groups from their respective shape types). However, when we look at the global t-test statistic, we see a higher significance in SA:V of the shapes against the reference sphere across the board indicating more viable shapes for experimentation.

**Table 4.** Unpaired two-sample t-tests performed on four groups and globally of the investigated polyhedra (4 from 6 for adequate test sample size): A: Platonic, B: Archimedes/Catalan, C: Kepler-Poinsot/Da Vinci, D: Wenninger, E: Global t-test. Critical SA:V denotes threshold of statistical significance in terms of SA:V (based on t-test statistic equation) as a rationale (asterisks) for choosing superior shapes within groups.

| Parameters (A.) | Shapes | Sphere (ref.) |
| --- | --- | --- |
| Mean | 1.04 | 0.6 |
| Variance | 0.22 | 0 |
| Observations | 5 | 5 |
| Hypothesized Mean Difference | 0 | |
| df | 4 | |
| t Stat | 2.07 | |
| P(T>=t) one-tail | 0.05 | |
| t Critical one-tail | 2.13 | |
| Critical SA:V | 1.05 | |

| Parameters (C.) | Shapes | Sphere (ref.) |
| --- | --- | --- |
| Mean | 3.04 | 0.6 |
| Variance | 5.98 | 0 |
| Observations | 5 | 5 |
| Hypothesized Mean Difference | 0 | |
| df | 4 | |
| t Stat | 2.23 | |
| P(T>=t) one-tail | 0.04 | |
| t Critical one-tail | 2.13 | |
| Critical SA:V | 2.93 | |

| Parameters (B.) | Shapes | Sphere (ref.) |
| --- | --- | --- |
| Mean | 0.66 | 0.6 |
| Variance | 0.01 | 0 |
| Observations | 7 | 7 |
| Hypothesized Mean Difference | 0 | |
| df | 6 | |
| t Stat | 1.46 | |
| P(T>=t) one-tail | 0.1 | |
| t Critical one-tail | 1.94 | |
| Critical SA:V | 0.68 | |

| Parameters (D.) | Shapes | Sphere (ref.) |
| --- | --- | --- |
| Mean | 4.7 | 0.6 |
| Variance | 50.02 | 0 |
| Observations | 5 | 5 |
| Hypothesized Mean Difference | 0 | |
| df | 4 | |
| t Stat | 1.3 | |
| P(T>=t) one-tail | 0.13 | |
| t Critical one-tail | 2.13 | |
| Critical SA:V | 7.34 | |

| Parameters (E.) | Shapes | Sphere (ref.) |
| --- | --- | --- |
| Mean | 2.21 | 0.6 |
| Variance | 13.48 | 0 |
| Observations | 22 | 22 |
| Hypothesized Mean Difference | 0 | |
| df | 21 | |
| t Stat | 2.05 | |
| P(T>=t) one-tail | 0.03 | |
| t Critical one-tail | 1.72 | |
| Critical SA:V | 1.95 | |

In addition to those elucidated by the bar graph figures, all but the Dodecadodecahedron and small ditrigonal icosidodecahedron from the concave group are statistically significant enough for consideration versus none of the shapes in the convex category, meeting the critical SA:V to declare it. Moreover, it is important to note that shapes shown in the "within group" t-tests elucidate this better than the global for the group as it pulls less weight in terms of the global significance. This fact applies inversely in the concave category since the group pulls the highest weight of significance, thereby giving importance to the "global" t-test for further elucidation.

The first assumption with the choice of the test type is that the sample size is adequate. The second assumption is that the data is assumed to possess normality due to experimenter's aiming for a mean size in a colloidal or nanofabricated batch of nanoparticles making the mean observation population based. The means calculated are from continuous or ordinal within the tests. The third assumption is the homogeneity of variance which is more difficult to ascertain based on multiple variables like the fabrication methods, material type, and researchers themselves. The second falls under the issues of the third assumption   as well when it comes to possible ascertainment issues. The fourth assumption is that the alpha at 0.05 is established as a decent parameter for the critical p-value. The fifth and final assumption is the choice of randomness. Arguably, the choice of 10 nm may be non-random as it is within the nano-regime and the assumed population

mean of a colloidal or batch nanoparticle solution but the variety of shapes and their unique calculations may give more credence to the assumption.

## 4. Conclusions

Only 10 out of 22 investigated shapes were significant in regard to the global t-test whereas only 7 out of 22 were seen as significant within the groups. Overall, without duplication, 14 out of 22 investigated shapes possessed significance when we only take into account the t-tests done within the convex groups helping its lack of effect in the global t-test and the global t-test indicating more significance in the concave group, showing how lower variance in potentially high significance in the groups can mar determining which shapes are best to investigate experimentally. The remaining were either on the cusp of significance or not at all, showing that some may offer a rationale behind their choice but it less likely, while others would show little to no efficacy at all. The shapes that possess this significance however warrant investigation in basic research for inorganic nanoparticles employing the best or most available methods for creating complex structures or molds from multiple processing methods. More complex and possibly efficacious morphologies may require more specialization in nanofabrication. Obviously, some may not be feasible to develop, but they could offer, in addition to the others, a possible novel open inquiry of investigation.

The state-of-the-art in nanotechnology is ever evolving and refining. This paper showcases one of those examples in regard to the morphological tuning of inorganic nanoparticles as a promising aspect of optimization in nanomedicine and nanotechnology itself. A refinement that acknowledges long-discovered aspects of advanced geometry, mathematical derivation/proofing, and computer programming further proves the uncanny ability for this field to be amenable and tenable to being interdisciplinary, which continues to serve it well.

**Supplementary Materials:** The following are available online at www.mdpi.com/xxx/s1

**Author Contributions:** Conceptualization, W.A.W., and D.J.D; methodology, W.A.W.; software, W.A.W.; validation, W.A.W.; formal analysis, W.A.W. A,D., P.R. ; investigation, W.A.W.; resources, W.A.W.; data curation, W.A.W.; writing—original draft preparation, W.A.W.; writing—review and editing, D.J.D. and S.S. M; visualization, W.A.W.; supervision, S.S.M.; project administration, S.S.M.; funding acquisition, S.S.M. All authors have read and agreed to the published version of the manuscript.

**Funding:** This research was supported by the Graduate Program Research Support to students, Taneja College of Pharmacy, University of South Florida. SSM is a Veteran Affairs Research Career Scientist (IK6BX003778) and his research is supported by a VA Merit Review Program (BX003685).

**Acknowledgments:** W.A.W. thanks Ashley Denslow and Peter Radulovic for their assistance with Python syntax and to Glärbo, from the Mathematics section of the website: Stack Exchange, who helped with the general SA and V derivations for certain unique polyhedra.

**Conflicts of Interest:** The authors declare no conflict of interest.

## References

[1] S. S. Mohapatra *et al.*, "Advances in Translational Nanotechnology: Challenges and Opportunities," *Appl. Sci.*, vol. 10, no. 14, p. 4881, Jul. 2020, doi: 10.3390/app10144881.

[2] M. D. Shin *et al.*, "COVID-19 vaccine development and a potential nanomaterial path forward," *Nat. Nanotechnol.*, vol. 15, no. 8, pp. 646–655, 2020, doi: 10.1038/s41565-020-0737-y.

[3] D. J. Denmark, X. Bustos-Perez, A. Swain, M. H. Phan, S. Mohapatra, and S. S. Mohapatra, "Readiness of Magnetic Nanobiosensors for Point-of-Care Commercialization," *Journal of Electronic Materials*, vol. 48, no. 8. Springer New York LLC, pp. 4749–4761, Aug. 15, 2019, doi: 10.1007/s11664-019-07275-7.

[4] D. J. Denmark *et al.*, "Inorganic nanoparticles for biomedicine: Where materials scientists meet medical

research," *Drug Deliv.*, vol. 24, no. 1, pp. 1317–1324, Jan. 2017, doi: 10.1016/j.mattod.2015.07.004.

[5]     D. J. Denmark *et al.*, "Photopolymerization-based synthesis of iron oxide nanoparticle embedded PNIPAM nanogels for biomedic _ Enhanced Reader.pdf," *Drug Deliv.*, vol. 24, no. 1, pp. 1317–1324, Jan. 2017, [Online]. Available: https://www.tandfonline.com/doi/full/10.1080/10717544.2017.1373164.

[6]     D. J. Denmark *et al.*, "Remote triggering of thermoresponsive PNIPAM by iron oxide nanoparticles," *RSC Adv.*, vol. 6, no. 7, pp. 5641–5652, Jan. 2016, doi: 10.1039/c5ra21617f.

[7]     Khodashenas, B., & Ghorbani, H. R. (2019). Synthesis of silver nanoparticles with different shapes. Arabian Journal of Chemistry, 12(8), 1823–1838. https://doi.org/10.1016/j.arabjc.2014.12.014

[8]     P. N. Navya and H. K. Daima, "Rational engineering of physicochemical properties of nanomaterials for biomedical applications with nanotoxicological perspectives," *Nano Converg.*, vol. 3, no. 1, p. 1, Dec. 2016, doi: 10.1186/s40580-016-0064-z.

[9]     Z. Nemati *et al.*, "Enhanced Magnetic Hyperthermia in Iron Oxide Nano-Octopods: Size and Anisotropy Effects," *J. Phys. Chem. C*, vol. 120, no. 15, pp. 8370–8379, 2016, doi: 10.1021/acs.jpcc.6b01426.

[10]    W. W. Zhaohui Wu, Shuanglei Yang, "Shape control of inorganic nanoparticles from solution," *R. Soc. Chem. Nanoscale*, no. 3, p. 61, 2015.

[11]    V. Thambi, A. Kar, P. Ghosh, D. Paital, A. R. S. Gautam, and S. Khatua, "Synthesis of Complex Nanoparticle Geometries via pH-Controlled Overgrowth of Gold Nanorods," *ACS Omega*, vol. 4, no. 9, pp. 13733–13739, 2019, doi: 10.1021/acsomega.9b01119.

[12]    Y. H. Lee *et al.*, "Creating two self-assembly micro-environments to achieve super crystals with dual structures using polyhedral nanoparticles," *Nat. Commun.*, vol. 9, no. 1, 2018, doi: 10.1038/s41467-018-05102-x.

[13]    J. Shen, M. Shafiq, M. Ma, and H. Chen, "Synthesis and surface engineering of inorganic nanomaterials based on microfluidic technology," *Nanomaterials*, vol. 10, no. 6, pp. 1–29, 2020, doi: 10.3390/nano10061177.

[14]    M. Ahmed, *Nanomaterial synthesis*. Elsevier Inc., 2020.

[15]    L. Polavarapu, S. Mourdikoudis, I. Pastoriza-Santos, and J. Pérez-Juste, "Nanocrystal engineering of noble metals and metal chalcogenides: Controlling the morphology, composition and crystallinity," *CrystEngComm*, vol. 17, no. 20, pp. 3727–3762, 2015, doi: 10.1039/c5ce00112a.

[16]    A. Biswas, I. S. Bayer, A. S. Biris, T. Wang, E. Dervishi, and F. Faupel, "Advances in top-down and bottom-up surface nanofabrication: Techniques, applications & future prospects," *Adv. Colloid Interface Sci.*, vol. 170, no. 1–2, pp. 2–27, 2012, doi: 10.1016/j.cis.2011.11.001.

[17]    Webb, Robert "Stella: Polyhedron Navigator," Symmetry: Culture and Science, Vol. 11, Nos. 1-4,          p231-268, 2000 (available online at http://www.software3d.com/PolyNav/PolyNavigator.php)

[18]    Cauchy, A. L. "Recherches sur les polyèdres." J. de l'École Polytechnique 9, 68-86, 1813.

[19]    Wenninger, M. J. (1971). Polyhedron Models. Cambridge University Press.

[20]    S. Torquato and Y. Jiao, "Dense packings of the Platonic and Archimedean solids," Nature, vol. 460, no. 7257, pp. 876–879, Aug. 2009, doi: 10.1038/nature08239.

[21]    Pacioli, L., & Marinoni, A. (1982). De divina proportione. Silvano.

[22]    Catalan, E. (1865). Mémoire sur la théorie des polyèdres (Vol. 24). Gauthier-Villars (Journal: l'École Polytechnique).